HEALTH AND MEDICINE

PD-L1$^+$ neutrophils contribute to injury-induced infection susceptibility

Ajitha Thanabalasuriar[1,2], Abby J. Chiang[3], Christopher Morehouse[1], Margarita Camara[1], Shonda Hawkins[4], Ashley E. Keller[1], Adem C. Koksal[3], Carolina S. Caceres[1], Aaron A. Berlin[5], Nicholas Holoweckyj[6], Virginia N. Takahashi[1], Lily Cheng[6], Melissa de los Reyes[6], Mark Pelletier[1], Andriani C. Patera[1], Bret Sellman[1], Sonja Hess[3], Marcello Marelli[3], Chelsea C. Boo[3], Taylor S. Cohen[1], Antonio DiGiandomenico[1]*

The underlying mechanisms contributing to injury-induced infection susceptibility remain poorly understood. Here, we describe a rapid increase in neutrophil cell numbers in the lungs following induction of thermal injury. These neutrophils expressed elevated levels of programmed death ligand 1 (PD-L1) and exhibited altered gene expression profiles indicative of a reparative population. Upon injury, neutrophils migrate from the bone marrow to the skin but transiently arrest in the lung vasculature. Arrested neutrophils interact with programmed cell death protein 1 (PD-1) on lung endothelial cells. A period of susceptibility to infection is linked to PD-L1$^+$ neutrophil accumulation in the lung. Systemic treatment of injured animals with an anti–PD-L1 antibody prevented neutrophil accumulation in the lung and reduced susceptibility to infection but augmented skin healing, resulting in increased epidermal growth. This work provides evidence that injury promotes changes to neutrophils that are important for wound healing but contribute to infection susceptibility.

INTRODUCTION

Approximately 300 burn-related patients are treated daily in emergency rooms, making these injuries one of the most common and devastating forms of trauma (*1*). One-third of these involve pediatric patients, and the risk for airway compromise and likelihood for intubation is increased in these subjects due to smaller airways and greater risk of closure from edema (*2*). Subjects with severe burns must be monitored for acute respiratory distress syndrome (ARDS) (*3*, *4*). ARDS leaves patients with burn injury with an increased risk of infection, specifically bacterial pneumonia (*1*). For these reasons, cutaneous burn wounds are a notable cause of death worldwide and require immediate specialized care to minimize morbidity and mortality (*5*).

Innate immune cells are pivotal participants in the body's reaction to physical trauma and injury (*6*). Apart from their traditional role in infection control, neutrophils play a crucial role in the healing and regeneration process (*7*, *8*). Recently, a distinct proangiogenic neutrophil population was identified in the circulation of humans and mice (*7*). Proangiogenic neutrophils release greater amounts of matrix metallopeptidase 9 (MMP9), which induces angiogenesis by degrading the extracellular matrix, promoting the release of matrix-bound vascular endothelial growth factor (VEGF) (*7*). Notably, if neutrophils are unable to move toward an injury site, the wound exhibits delayed re-epithelialization due to an altered collagen matrix (*9*, *10*).

Following injury, resident cells release inflammatory cytokines and chemokines to recruit reparative neutrophils to the injury site. Excess inflammation, however, can result in undesired tissue damage. Therefore, the body's ability to control inflammation is tightly regulated. One of the most studied regulators is programmed death ligand 1 (PD-L1) and programmed cell death protein 1 (PD-1) immune checkpoint pathway, which prevents excessive tissue destruction during inflammation (*11*). PD-L1 is expressed by multiple cell types, and expression is induced by numerous proinflammatory factors. During sepsis, PD-L1 expression on neutrophils increases with inflammation and correlates with impaired antibacterial function (*11*, *12*). Targeting PD-L1 with blocking antibodies can also enhance neutrophil innate immune function (*12*–*14*). In addition, PD-L1 pathways were shown to be important in wound healing (*15*). Exosomal PD-L1 has been shown to promote skin cell migration and wound healing (*15*).

In this study, we use a model of thermal injury in which mice become sensitive to bacterial infection for a period of time following injury. We identify a population of neutrophils that transiently increase expression of PD-L1 following thermal injury. These neutrophils are retained in the lung following the insult, correlating with a period of increased susceptibility of animals to bacterial infection. We also demonstrate that PD-L1 expression is dependent on transforming growth factor–β (TGF-β) signaling. Systemic blocking of either PD-L1 or TGF-β using antibody therapies reduces the neutrophil burden in the lung and protects the animals from infection. Neutralization of TGF-β, but not PD-L1, promoted wound healing following injury. This work describes an immune regulatory pathway through which the host promotes proper wound healing, at the price of increasing susceptibility to respiratory infection.

RESULTS

Cutaneous burn injury leads to expansion of PD-L1$^+$ neutrophils systemically

We have developed a murine dorsal thermal injury model in which animals receive a 12 to 15% total body surface area injury (fig. S1A). Although pathological assessment confirms that these are indeed

[1]Microbial Sciences, Biopharmaceuticals R&D, AstraZeneca, Gaithersburg, MD, USA. [2]McGill University, Department of Pharmacology and Therapeutics, Faculty of Medicine, Montreal, QC Canada. [3]Dynamic Omics, Antibody Discovery and Protein Engineering (ADPE), R&D, AstraZeneca, Gaithersburg, MD, USA. [4]Animal Sciences and Technologies, Clinical Pharmacology and Safety Sciences, AstraZeneca, Gaithersburg, MD, USA. [5]Respiratory and Immunology, Biopharmaceuticals R&D, AstraZeneca, Gaithersburg, MD, USA. [6]Research and Early Development, Oncology R&D, AstraZeneca, Gaithersburg, MD, USA.
*Corresponding author. Email: antonio.digiandomenico@astrazeneca.com

third-degree burns, mice can effectively heal without requiring skin grafts (Fig. 1, A and B). Injured murine skin progressively heals over time, and the injury site can reduce in size by 60% and even resume hair growth by 30 days after injury (Fig. 1C). Thus, this model would be representative of second-degree burns in humans (*16*). To understand how cutaneous burn injury affects the immune system, we evaluated release of cytokines and chemokines in serum from injured mice (Fig. 1D). We observed a transient increase in anti-inflammatory cytokines, particularly interleukin-10 (IL-10), at 3 hours after injury; by 72 hours after injury, expression of IL-10 was similar to noninjured levels (Fig. 1D). The increase in IL-10 corresponded with a spike in TGF-β levels (Fig. 1E). Moreover, there was a marked increase in chemokines detected in the blood, such as keratinocyte-derived chemokine (KC) and macrophage inflammatory protein 2 (MIP-2), which were elevated in serum by 3 hours after injury and returned to basal levels by 72 hours (Fig. 1, D, F, and G). The increase in KC corresponded with increased recruitment of neutrophils into the blood (Fig. 1H).

Following burn, increased expression of the transmembrane protein PD-L1 was observed on neutrophils (Fig. 1I), whereas similar increases were not observed on other analyzed cells in the blood (fig. S2, A and B). Expression of PD-L1 by neutrophils in blood was transient and unrelated to neutrophil death, peaking 3 hours after injury and returning to basal levels by 48 hours (Fig. 1I and fig. S1B). Systemic, but not bone marrow, neutrophil expression of PD-L1 correlated with TGF-β levels, consistent with prior reports of TGF-β regulating neutrophil phenotype [Fig. 1, E and I, and fig. S1C; (*17*)].

Thermal injury promotes pulmonary neutrophil accumulation

Patients with burn wound are susceptible to ARDS, which is characterized by severe respiratory distress, hypoxemic respiratory failure refractory to oxygen administration, and pulmonary edema that is not the result of congestive heart failure or fluid overload (*18*, *19*). In addition, a hallmark of ARDS is increased leukocyte infiltration into the lungs, particularly neutrophils (*19*). We assessed the lungs of thermally injured mice to determine whether they experienced an ARDS-like phenotype. Similar to the systemic response, we observed an anti-inflammatory cytokine profile (IL-10 and IL-4) in

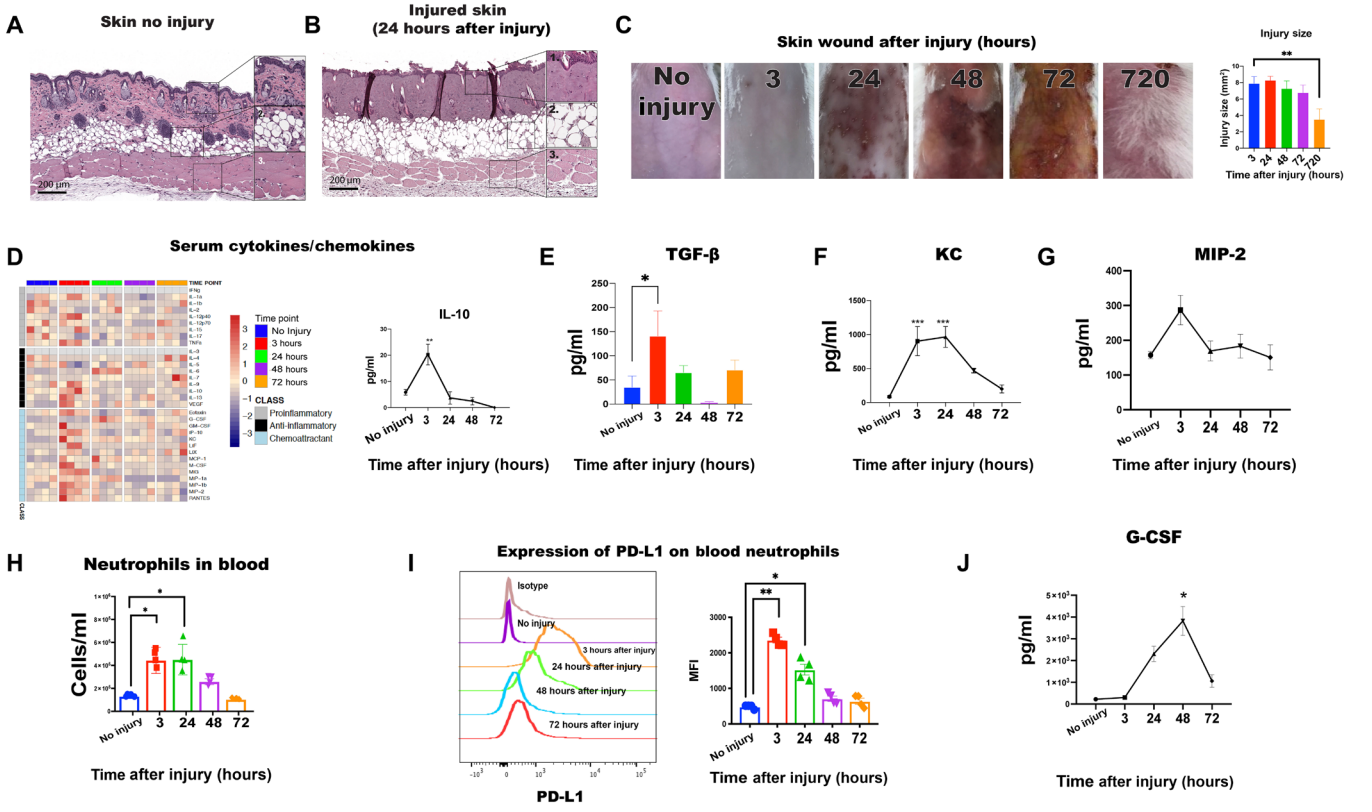

Fig. 1. Thermal injury causes systemic changes to the body. (**A**) Hematoxylin and eosin (H&E)–stained skin sections of mouse skin after removing the fur. Histology representing normal skin (×10 magnification); insets (×20 magnification) show epidermis and dermis with adnexal structures (1), adipose layer (2), and muscle layer (3). (**B**) H&E-stained skin sections of a mouse that had its fur removed and skin injured. Histologic confirmation of third-degree thermal injury (×10 magnification); insets (×20 magnification) show full-thickness thermal damage only of the epidermis and dermis (1) and do not extend to the adipose (2) or muscle layer (3). (**C**) Gross morphological changes after thermal injury to the skin at indicated time points. (**D**) Systemic cytokine and chemokine profile was evaluated in mouse serum after injury using Luminex. Data in heatmaps were plotted as *Z* score. (**E**) Enzyme-linked immunosorbent assay (ELISA) was used to quantify TGF-β in mouse serum after injury. (**F**) Quantification of chemokine KC in serum. (G) Quantification of chemokine MIP-2 in serum. (**H**) Flow cytometric analysis used to assess neutrophil recruitment in blood. (**I**) Flow cytometry was used to assess PD-L1 expression on neutrophils. MFI, mean fluorescence intensity. (**J**) Quantification of chemokine granulocyte colony-stimulating factor (G-CSF) in serum. All experiments were repeated three times ($N = 4$), a single experimental repeat is represented in the figure, and experiments were analyzed using Brown-Forsythe and Welch analysis of variance (ANOVA) test, unless otherwise indicated. One-way ANOVA analysis was performed for colony-forming unit (CFU) data with nonparametric Kruskal-Wallis test. $^{*}P < 0.05$, $^{**}P < 0.05$, and $^{***}P < 0.0001$.

the lungs; however, peak expression was observed at 24 hours rather than at 3 hours after injury (Figs. 1D and 2A).

Flow cytometric analysis of lung tissue revealed significantly increased neutrophil recruitment to the lung, which peaked 24 hours after injury (Fig. 2B). Similarly, intravital imaging revealed neutrophil clustering in the lung vasculature of injured animals when compared with noninjured animals (Fig. 2, C and D, and movie S3), which was associated with decreased lung function as quantified by airway resistance (lung pressure divided by airflow; Fig. 2E). Lung neutrophils also displayed markers characteristic of activation, such as increased Cd11a and Cd11b expression (fig. S3, A and B). We did not observe evidence of neutrophil extracellular trap (NET) formation by enzyme-linked immunosorbent assay (ELISA) or proteomics analyses (fig. S3, C and D). Unlike the lung, we did not observe evidence of PD-L1$^+$ neutrophil accumulation in other tissues, such as the spleen and liver, at various times after injury (fig. S2, C to F).

Bronchoalveolar lavage (BAL) of injured animals did not yield a similar increase in neutrophils compared with noninjured animals, suggesting that the cells are trapped within the lung vasculature (fig. S2G). Consistent with this hypothesis, neutrophils stained in the bloodstream were positive with an anti-CD45 antibody when administered intravenously (Fig. 2F).

Neutrophils in injured mice are long lived and have increased expression of reparative genes

Following injury, lung-recruited neutrophils showed significant phenotypic differences from steady state. This included changes in behavior and expression of PD-L1, CD47, and CXCR4 (movie S3, Fig. 2G, and fig. S3E). Expression of PD-L1 on lung neutrophils peaked at 3 and 24 hours, returning to preinjury levels by 48 hours (Fig. 2G). Neutrophils in the spleen and liver did not exhibit evidence of increased PD-L1 expression (fig. S2, C and D). We also did not observe increases in cell numbers or PD-L1 expression on alveolar macrophages after injury (fig. S2, H and I). Neutrophil CD47 and CXCR4 expression peaked at 24 hours, returning to baseline at 48 hours (fig. S3E). CD47 acts as a "don't eat me" signal and suggests

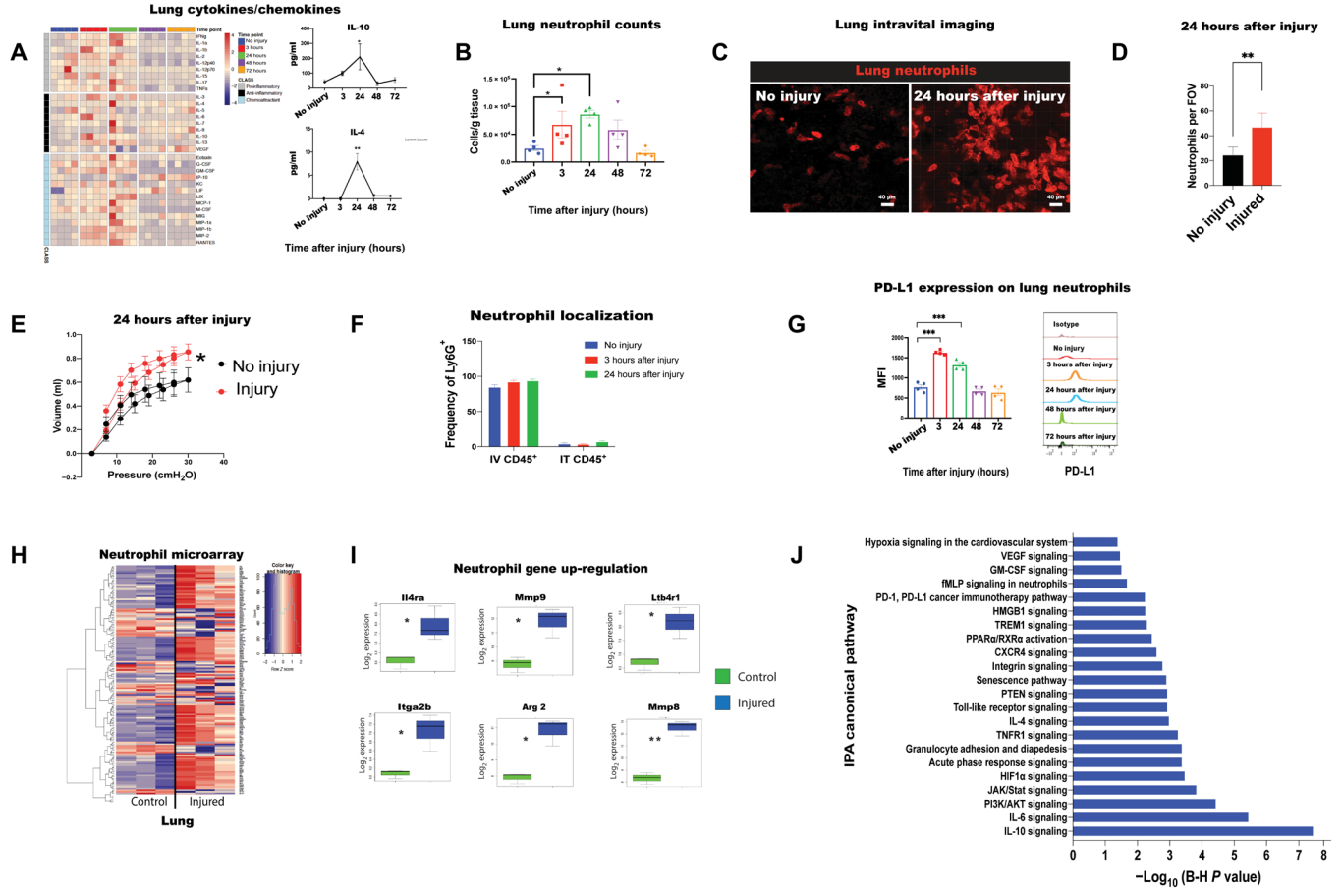

Fig. 2. Thermal injury causes changes to lung cytokine profiles and airway distress. (**A**) Luminex analysis of secreted cytokine/chemokine profile in the lung bronchial lavage fluid. Heatmap shows the data after *Z* score. Raw data of IL-10 and IL-4 from Luminex are shown in the line plots. (**B**) The number of lung neutrophils was assessed by flow cytometry at various time points after injury. (**C**) Representative intravital image of lung neutrophils in noninjured and 24 hours postinjured mice. Neutrophils were stained with Ly6G 1A8 antibody (red). (**D**) Quantification of neutrophils by intravital microscopy. FOV, field of view. (**E**) Pressure-volume curve to assess lung inflation and breathing in mice. (**F**) CD45$^+$ antibody was administered intravenously (IV) or intratracheally (IT). Quantification of CD45$^+$ and Ly6G$^+$ cells. (**G**) PD-L1 expression on lung neutrophils assessed by flow cytometry. (**H**) Microarray analysis of mRNA extracted from neutrophils harvested from mouse lungs and blood 45 min after injury. Gene list and gene expression data are found in table S2. (**I**) Differentially expressed genes of interest found in microarray analysis of lungs. (**J**) Ingenuity Pathway Analaysis (IPA) based on Microarray data. Graph depicts most significantly up-regulated gene pathways in neutrophils harvested from injured mice. All experiments were repeated three times, $N = 4$ per experimental group unless otherwise indicated. A single experimental repeat is represented in the figure. One-way ANOVA analysis was performed for CFU data with nonparametric Kruskal-Wallis test. For all other data, Brown-Forsythe and Welch ANOVA test was performed. Error bars represent SD unless otherwise noted. *$P < 0.05$, **$P < 0.05$, and ***$P < 0.0001$.

that these cells were avoiding efferocytotic killing and clearance (*20*). In addition, CXCR4 expression is thought to serve as a depriming step as neutrophils move through injury sites, promoting resolution of inflammation (*21*).

We hypothesized that neutrophils in injured mice were phenotypically distinct from uninjured mice. To evaluate this hypothesis, we isolated neutrophils from the lungs of noninjured and injured animals followed by microarray to monitor overall changes in gene expression profiles (Fig. 2H). After tissue damage, damage-associated molecular patterns (DAMPs) signal for early neutrophil recruitment (*9*). DAMPs released from damaged cells activate surrounding tissues and induce the production of chemokines and lipid mediators, such as leukotriene B4, which is a strong inducer of neutrophil chemotaxis toward injury (*22*). Expression of *ltrb4* was increased in neutrophils isolated from the lungs of injured animals (Fig. 2I). *MMP9*, *IL-4* receptor, and Arginase 2, markers for N2-like neutrophils, were also increased after injury. *Itga2b* and *Mmp8*, genes induced by TGF-β, are up-regulated in the lung neutrophils after thermal injury, further corroborating the role of TGF-β in promoting neutrophil phenotype change (Fig. 2H) (*23*). TGF-β gene was not up-regulated in neutrophils after injury, suggesting an alternate cellular source (fig. S4A). In addition, pathway analysis of neutrophils from injured mice showed significant up-regulation of anti-inflammatory and PD-L1 pathways, further corroborating our flow cytometry data (Fig. 2J). Using proteomics and ELISA, we detected increased TGF-β levels in the serum 3 hours after injury (Fig. 1E and fig. S4B). It is likely that neutrophils are being primed by systemic TGF-β before they move to the skin to perform reparative function.

Pulmonary neutrophil accumulation marks increased vascular permeability and increased susceptibility to infection after thermal injury

Pseudomonas aeruginosa is an important cause of infections in patients with burn injury, and thermally injured mice are known to be highly susceptible to infection with this opportunistic bacterium (*24*). In our model, we found that injured mice exhibited increased susceptibility to intranasal infection with *P. aeruginosa* between 3 and 24 hours after burn (Fig. 3, A and B). Intriguingly, mice that were infected at 48 or 72 hours after injury showed limited to no susceptibility to infection (Fig. 3, A and B). Survival also correlated with PD-L1 expression on neutrophils, which peaked between 3 and 24 hours after injury (Fig. 2G). We next evaluated bacterial burden levels at the site of infection and distally in the spleen. Infection of injured mice with *P. aeruginosa* resulted in 4- and 3-log higher colony-forming units (CFUs) in the lung and spleen, respectively, when compared with noninjured mice, exemplifying an inability to control infection and the ability of the bacteria to disseminate throughout the body (Fig. 3, C and D). Similar results were observed when mice were infected with *Staphylococcus aureus* and *Klebsiella pneumoniae*, two additional pathogens commonly seen in intensive care units to cause pneumonia, sepsis, and death in immune-compromised individuals (Fig. 3, E and F).

The appearance of bacteria in the spleen suggested that cutaneous thermal injury causes significant disruption to the lung's epithelial and endothelial barriers, potentially resulting in increased vascular leakage. These results were confirmed following intravenous administration of Evans blue dye, which effectively leaked into the lung parenchyma in injured animals (Fig. 3G). Moreover, through intravital imaging, we found that 70-kDa tetramethyl rhodamine isothiocyanate (TRITC)–dextran effectively leaked into the lung parenchyma after thermal injury (Fig. 3H). Enhanced permeability of the endothelia is likely due to the increased number of neutrophils in the lung vasculature (Fig. 2, B and C). As these neutrophils cluster in the lung, they may maintain enzymatic activity, expressing molecules such as MMP9 and MMP8 (Fig. 2I). These enzymes can facilitate breakdown of components within the endothelial wall, increasing vascular permeability.

Once bacteria pass through the endothelial barrier, they are able to disseminate throughout the body. To determine whether the innate immune defect was restricted to the lung, we intravenously infected mice with *P. aeruginosa*. We used a bacterial inoculum that yielded approximately 80% survival in noninjured mice and found that injured animals were more susceptible to infection at 3 and 24 hours after injury, suggesting that increased sensitivity to respiratory infection was not simply due to loss of lung barrier function (Fig. 4, A and B). Animals infected at 48 or 72 hours after injury exhibited similar susceptibility to *P. aeruginosa* infection as noninjured animals (Fig. 4, A and B). We observed an increase in bloodstream CFU at 17 hours after infection when compared with noninjured animals (Fig. 4C). These uncleared bacteria disseminated from the blood to the liver and spleen, with the highest CFU per gram found in the lung tissue (fig. S1E). It has been previously noted that sepsis results in ARDS; given that the injury itself is likely causing an ARDS-like phenotype, it could be that the bacteriemic infection is exacerbating respiratory distress in these mice, resulting in death (*25*).

We evaluated how neutrophils from thermally injured animals behaved in the presence of *P. aeruginosa* using intravital imaging to observe interactions in real time. Unexpectedly, neutrophils from injured mice exhibited enhanced bacterial phagocytosis of *P. aeruginosa* (Fig. 4, D and E, and movies S1 and S2). Ex vivo analysis of neutrophils by flow cytometry from infected mice also showed similar trends as intravital microscopy. Injured mice showed increased frequency of neutrophils with intracellular bacteria compared with neutrophils from noninjured mice (Fig. 2F). We observed an increase in neutrophil death in injured and infected mice, which was not observed in noninjured and infected animals at this time point (Fig. 4, G and H). These results suggest that although neutrophils in injured animals are effective at phagocytosing bacteria, they are unable to mediate bacterial killing. In this process of phagocytosing bacteria and dying, neutrophils could result in overt inflammation. Luminex analysis of cytokines in injured and infected mice showed a spike in cytokines and chemokines in injured and infected animals, which was notable relative to infected uninjured animals (Fig. 4I).

Neutrophils arrest in the lung in a PD-L1–dependent manner

Neutrophils are known to be important for tissue healing; therefore, we monitored neutrophil trafficking to the skin, the site of thermal injury (*7*). We performed flow cytometry on cells recovered from the bone marrow, blood, lungs, and skin at various time points after injury (Fig. 5, A to D). We found that neutrophils are released from the bone marrow at 3 and 24 hours after injury as indicated by decreased neutrophils in the bone marrow at these times (Fig. 5A and fig. S4C). This is intriguing as we do not observe an increase in granulocyte colony-stimulating factor (G-CSF) until 24 hours after injury, but we did observe an increase in MIP-2 at 3 hours after injury (Fig. 1, G and J). These data suggest that thermal injury induces a

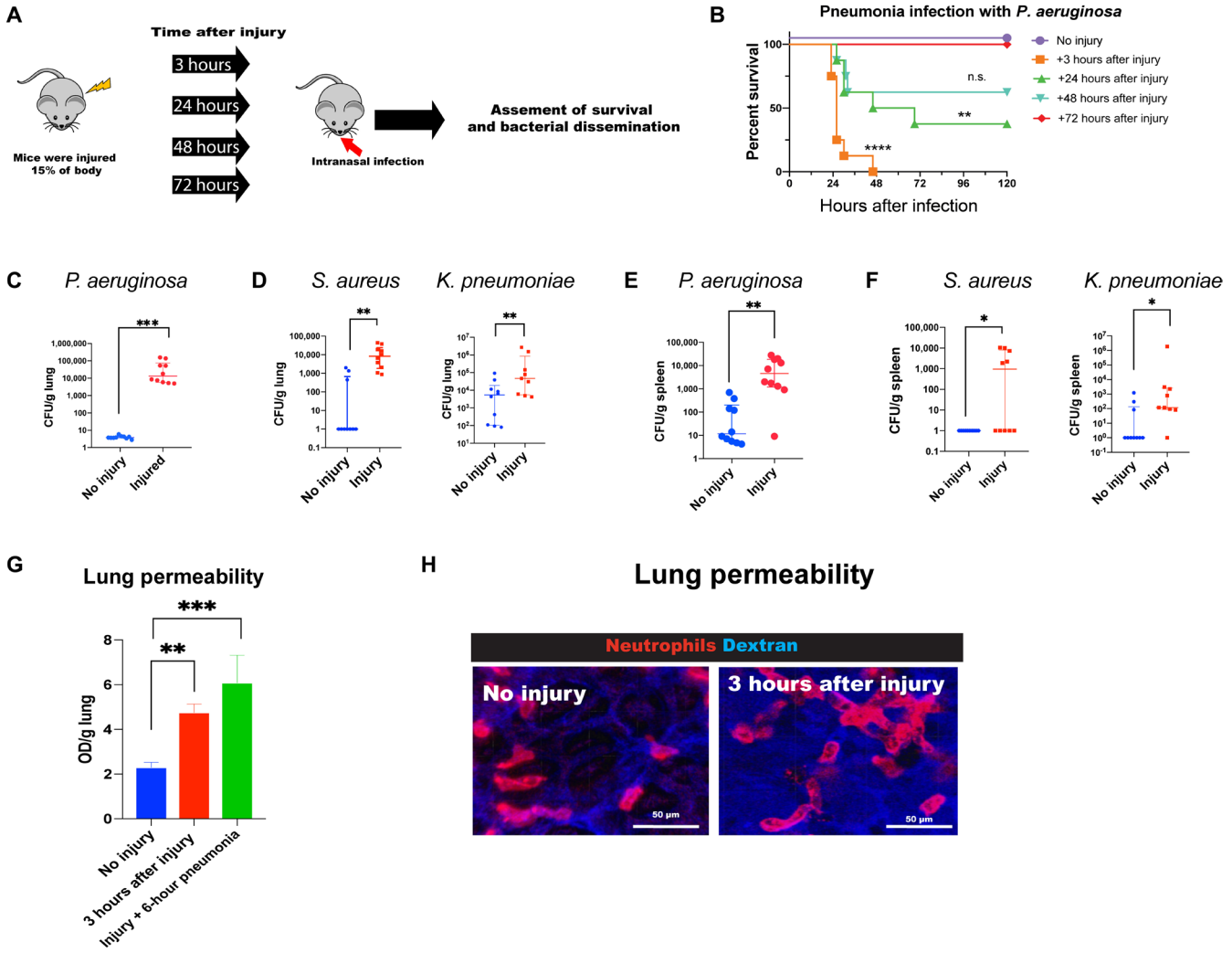

Fig. 3. Thermally injured mice are susceptible to intranasal infection at 3 and 24 hours after injury because of increased vascular permeability. (**A**) Schematic representation of how mice were injured and infected. (**B**) Survival curve of injured mice infected intranasally with *P. aeruginosa*. Survival curve analysis was performed with Gehan-Breslow-Wilcoxon test, and error bars represent 95% confidence interval. n.s., not significant. (**C**) CFUs of *P. aeruginosa* in injured mice infected at 3 hours after injury. CFUs were evaluated at 24 hours after infection in the lung. (**D**) The CFUs of *Staphylococcus aureus* and *Klebsiella pneumoniae* in injured mice infected at 3 hours after injury. CFUs were evaluated at 24 hours after infection in the lung, $N = 10$. (**E**) The CFUs of *P. aeruginosa* in injured mice infected at 3 hours after injury. CFUs were evaluated at 24 hours after infection in the spleen, $N = 10$. (**F**) CFUs of *S. aureus* and *K. pneumoniae* in injured mice infected at 3 hours after injury. CFUs were evaluated at 24 hours after infection in the spleen. Data are represented as mean with interquartile range, $N = 10$. G. Evans blue was used to determine vascular permeability in the lung. (**H**) The lung intravital imaging showed neutrophils (Ly6G 1A8; red) and dextran (70-kDa TRITC-dextran; blue). TRITC-dextran (70 kDa) is seen in blue. All experiments were repeated three times ($N = 4$) unless otherwise indicated. A single experimental repeat is represented in the figure. One-way ANOVA analysis was performed for CFU data with nonparametric Kruskal-Wallis test. For all other data, Brown-Forsythe and Welch ANOVA test was performed. Error bars represent SD. *$P < 0.05$, **$P < 0.05$, and ***$P < 0.0001$.

potent release of neutrophils from the bone marrow, exhausting neutrophil pools and resulting in initiation of granulopoiesis indicated by increased G-CSF at 24 hours after injury. Neutrophils released from the bone marrow accumulated in the blood and lungs of mice but were not observed in the spleen or liver (Fig. 5, A to D, and fig. S2, E and F). Forty-eight hours after injury, neutrophils decreased in the blood and lungs and began to increase in the skin (Fig. 5, B to D).

Given the increase in PD-L1 expression on lung neutrophils and the observation that these cells accumulated in the lung, we hypothesized that increased binding to its cognate receptor, PD-1, may explain this phenomenon. To test this, we assessed PD-1 expression on several cell types, including T and B cells. Increased PD-1 expression was only observed on lung endothelial cells after thermal injury (fig. S2, J to L, and Fig. 5, E and F). To confirm whether neutrophil accumulation in the lung was due to PD-L1/PD-1 interaction, we evaluated the fate of neutrophils in injured animals treated with an anti–PD-L1 monoclonal antibody (mAb), PD-L1 clone 20.6 (Fig. 5G). Using homogeneous time-resolved fluorescence (HTRF) assays, we found that our anti–PD-L1 mAb blocked PD-1/PD-L1 interactions but not PD-L1 CD80 interactions (fig. S4D). In addition, TGF-β neutralization resulted in reduced expression of PD-L1 on lung neutrophils and PD-1 on lung endothelial cells [Fig. 5, H to J; (*26*)]. While anti–PD-L1 and anti–TGF-β treatment did not alter

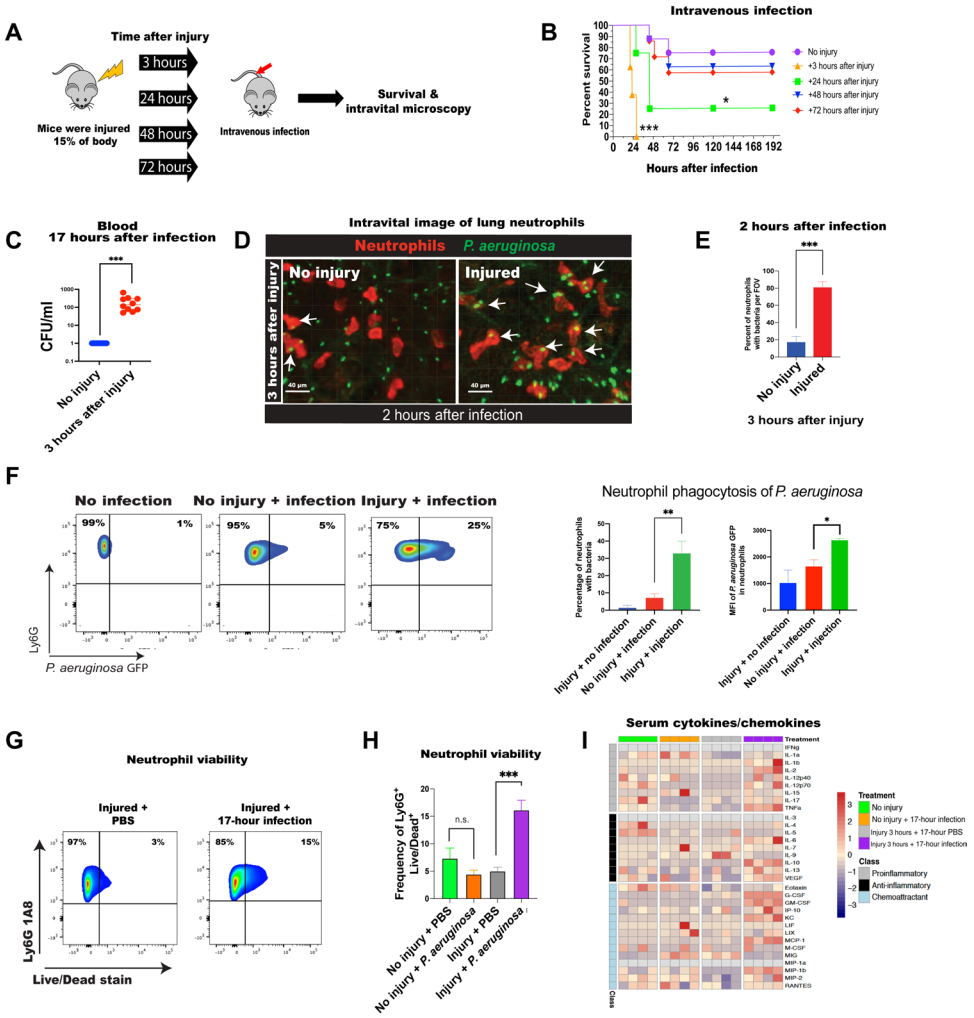

Fig. 4. Thermal injury causes increased susceptibility to bacteremic infections. (**A**) Schematic representation of how mice were injured and infected. (**B**) Survival curve of mice after injury and infection, $N = 7$. Error bars represent 95% confidence interval, and Gehan-Breslow-Wilcoxon statistical test was performed. (**C**) Bacterial (CFU) assessed in blood at 17 hours after infection. Data are represented as mean with interquartile range, $N = 12$. (**D**) Intravital microscopy of lung 3 hours after injury and 2 hours after infection with *P. aeruginosa* (GFP). Neutrophils are stained with a Ly6G antibody and shown in red. *P. aeruginosa* is shown in green. White arrows point to neutrophils overlapping with bacteria. (**E**) Quantification of intravital image. (**F**) Ex vivo quantification of lung neutrophil phagocytosis of *P. aeruginosa*. Percentage neutrophils harvested from the lung that were positive for GFP *P. aeruginosa* were quantified, and the mean fluorescence of GFP in neutrophils was quantified. (**G**) Neutrophil viability after injury and infection was quantified using flow cytometry. (**H**) Quantification of neutrophil viability in injured and noninjured mice. (**I**) Cytokine/chemokine profiles in serum of injured and infected mice compared with noninjured and infected mice. $^*P < 0.05$, $^{**}P < 0.05$, and $^{***}P < 0.0001$. All experiments were repeated three times ($N = 4$), representative experiment is presented in the figure, and Brown-Forsythe and Welch ANOVA test was performed on data, unless otherwise indicated. Error bars represent SD. One-way ANOVA analysis was performed for CFU data with nonparametric Kruskal-Wallis test, and data are plotted as mean with interquartile range.

neutrophil numbers in the blood, it significantly reduced neutrophil numbers in the lung (Fig. 6, A to D). IL-10–neutralizing antibody was tested as a control because IL-10 was increased in mouse lungs and serum after injury (Figs. 1D and 2A). However, IL-10 treatment did not affect neutrophil recruitment to the lung after injury (fig. S4E). These data suggest that neutrophil PD-L1 interacts with epithelial PD-1, effectively arresting migration of these cells in the lung.

Blocking the TGF-β/PD-L1 axis reduces pulmonary dysfunction and increases survival after infection

We noted that anti–PD-L1 treatment of injured animals decreased lung neutrophil recruitment and clustering while also improving lung function compared with control antibody-treated mice (Fig. 6, A to E). Because neutrophil arrest in the lung correlated with increased susceptibility to infection, we hypothesized that anti–PD-L1 treatment would increase survival following infection. Mice were prophylactically treated with anti–PD-L1, anti–TGF-β, or anti–IL-10 antibodies before injury. Mice treated with anti–PD-L1 and anti–TGF-β mAbs showed significant improvements to survival after *P. aeruginosa* infection (Fig. 6, F and G). Similarly, mice infected intravenously showed significant improvement to anti–PD-L1 and anti–TGF-β therapy (fig. S4F). In contrast, mice treated with IL-10–neutralizing antibody did not reduce neutrophil accumulation in the lung or improve survival following infection (Fig. 6G and fig. S4E).

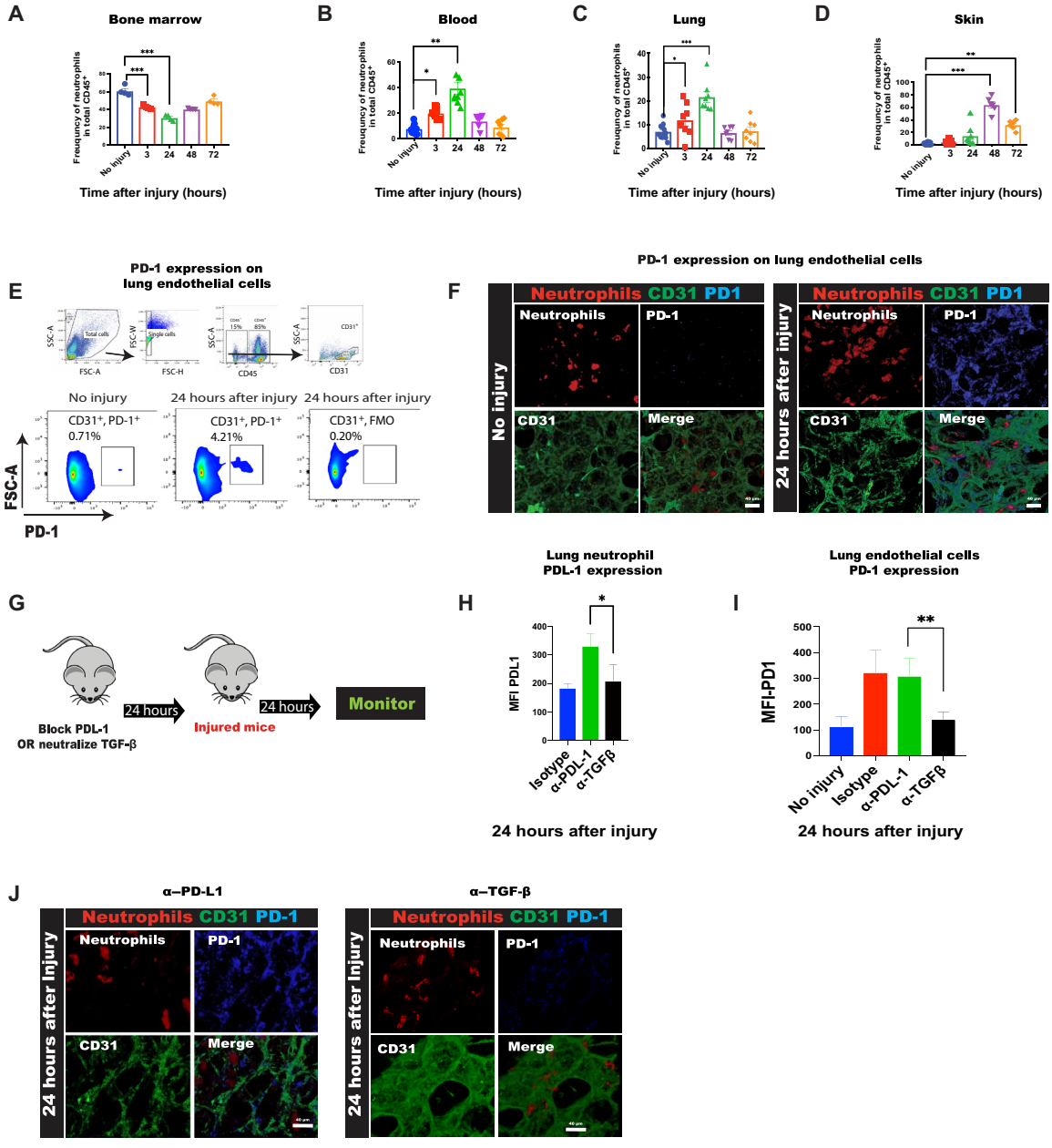

Fig. 5. PD-1 is expressed on endothelial cells. Flow cytometric analysis of neutrophils in (**A**) bone marrow, (**B**) blood, (**C**) lung, (**D**) skin in mice with no injury, and at various time points after injury. (**E**) Flow cytometric analysis of PD-1 expression on lung endothelial cells. SSC-A, side scatter area; FSC-A, forward scatter area; FSC-H, forward scatter height; FSC-W, forward scatter width. (**F**) Whole-mount images of lungs stained for neutrophils (Ly6G 1A8; red), endothelium (CD31; green), and PD-1 (blue). (**G**) Schematic representation of PD-L1 and TGF-β antibody treatment. (**H**) PD-L1 expression on neutrophils assessed by flow cytometry. (**I**) Quantification of PD-1 expression on endothelial cells of noninjured and injured mice treated with antibodies. (**J**) PD-1 expression on endothelium visualized by whole-mount staining of the lung in mice treated with either PD-L1 or TGF-β antibody. PD-1 (blue), neutrophils (red), and CD31 (endothelial cells; green). All experiments were repeated three times ($N = 4$), and representative experiment is presented in the figure. One-way ANOVA with Brown-Forsythe and Welch ANOVA test was performed. Error bars represent SD. α represents anti-, which protein the antibody is targeting. *$P < 0.05$, **$P < 0.05$, and ***$P < 0.0001$.

TGF-β neutralization and PD-L1 blocking have divergent effects on the healing process

Because PD-L1 and TGF-β blocking prevented neutrophils from accumulating in the lungs, we hypothesized that neutrophils might traffic more rapidly to the skin. We blocked PD-L1 or TGF-β in injured mice and looked at neutrophil infiltration to the skin and ability of the skin to heal (Fig. 7A). Neutrophils were recruited in higher numbers to the skin in injured mice treated with PD-L1–blocking mAb compared with isotype controls (Fig. 7B). Twenty-four hours after injury, if there are a higher number of recruited neutrophils in skin, as seen in anti–PD-L1–treated mice, there is a spike in VEGF (Fig. 7C). These data indicate that neutrophil recruitment to the skin is essential in healing, as VEGF is an important molecule for angiogenesis in both epithelial and endothelial cells (*27*). TGF-β neutralization had reduced neutrophils adhered to the lung vasculature, but when we quantified neutrophil numbers in the skin, we

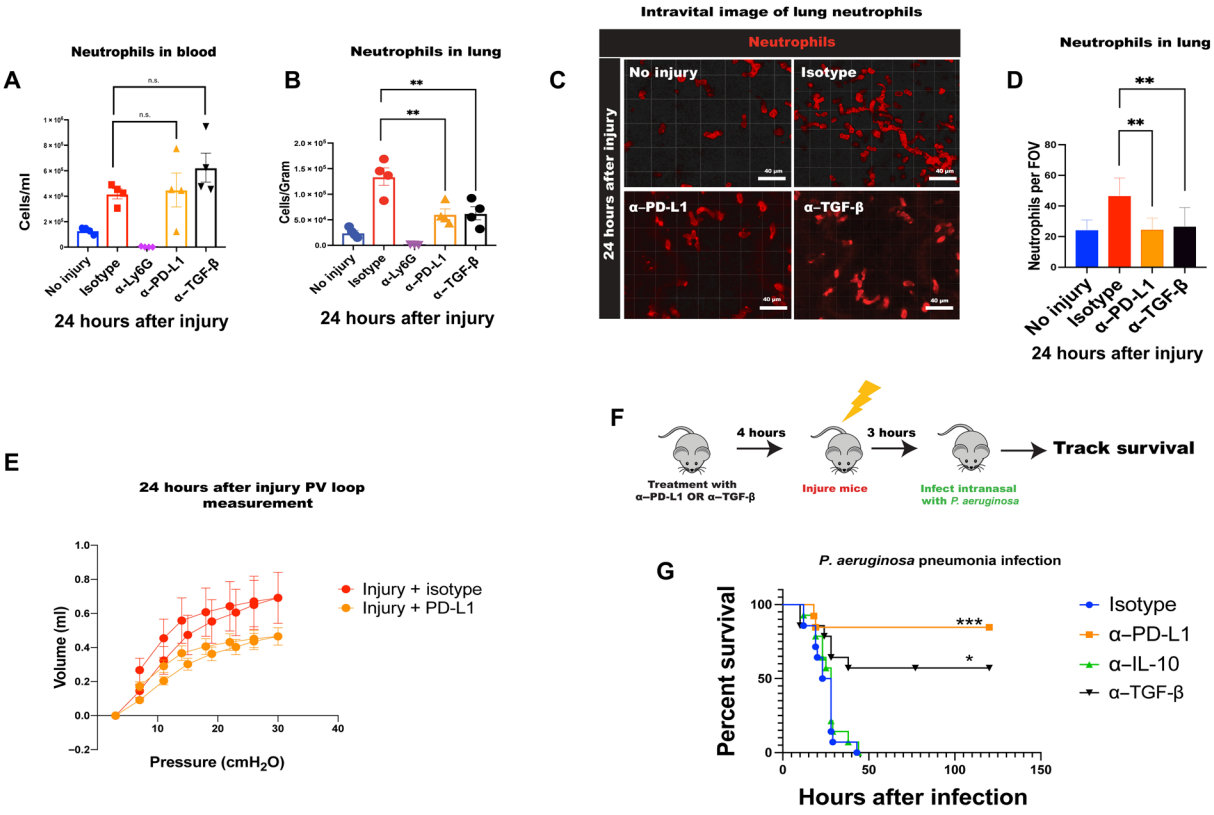

Fig. 6. Blocking PD-L1 reduces airway inflammation and dysfunction. (**A**) Quantification of neutrophils in the blood of noninjured and injured mice treated with antibodies. (**B**) Quantification of neutrophils in the lung of noninjured and injured mice treated with antibodies. (**C**) Still images captured from intravital videos of the lungs. Neutrophils are seen in red. (**D**) Quantification of intravital images of lung neutrophils. (**E**) Pressure-volume curve to assess lung inflation and breathing in mice. (**F**) Schematic of how survival experiments were performed. (**G**) Survival assessment of mice infected with *P. aeruginosa*. Survival curve analysis was performed with Gehan-Breslow-Wilcoxon test, and error bars represent 95% confidence interval. All experiments were repeated three times ($N = 4$), and representative experiment is presented in the figure. One-way ANOVA with Brown-Forsythe and Welch ANOVA test was performed. Error bars represent SD. α represents what protein the antibody used is targeting. $^{*}P < 0.05$, $^{**}P < 0.05$, and $^{***}P < 0.0001$.

did not observe a significant increase (Fig. 7B). Intriguingly, in TGF-β neutralization, we did observe increased neutrophil numbers in the bone marrow (fig. S4G). These data indicate a role for TGF-β signaling and PD-L1 expression in trafficking of neutrophils to the skin.

We then analyzed the healing in the skin in mice treated with anti–PD-L1 or anti–TGF-β by analyzing gross healing 30 days after injury and visualizing the collagen matrix of the skin 24 hours after injury. To confirm a role for neutrophils in the healing process, we treated mice with Ly6G-depleting antibody. These mice were unable to heal their wound, correlating with limited collagen deposition 24 hours after injury (Fig. 7, D and F). Anti–PD-L1–treated mice showed excessive scar formation and epidermal growth, likely due to excessive VEGF production, which can promote angiogenesis (Fig. 7, F to H). When we assessed collagen deposition, we observed increased irregularly shaped collagen fiber buildup in anti–PD-L1–treated mice, and the collagen appeared to be much thinner (Fig. 7, D and E). TGF-β–treated mice appeared similar to isotype control and did not present with excess or reduced epidermal growth (Fig. 7, F to H). Anti–TGF-β–treated mice exhibited collagen fiber thickness similar to mice with no injury at 24 hours after injury (Fig. 7E). These data suggest that PD-L1 and TGF-β play a similar role in the innate immune response following thermal injury in the lung. Conversely, they have additional functions in the context of wound healing, as inhibition of PD-L1 is detrimental to wound healing, while reducing TGF-β promotes proper collagen deposition and did not cause excessive scar formation. Together, these data suggest that by preventing PD-L1–dependent accumulation of neutrophils in the lung, airway distress and susceptibility to infection are reduced at the cost of proper wound healing (Fig. 8).

DISCUSSION

Burn injuries have complex pathological effects that can influence systemic host functions. Shortly after thermal injury, the patient's immune system undergoes several changes that may have severe consequences. However, to date, these changes are poorly understood. Burn injury has been associated with ARDS, resulting in patients having difficulty breathing, requiring ventilation, and therefore being at increased risk of ventilator-associated pneumonia. The risk of infections caused by multidrug-resistant bacterial pathogens increases with hospital length of stay in patients with burn injury (*1*). Therefore, a proactive infection control approach is essential in burn units. In this study, we identify a neutrophil subset central to the balance between healing and infection control after cutaneous burn injury and identify potential pathways that may be therapeutically targeted to prevent infection in patients with burn injury.

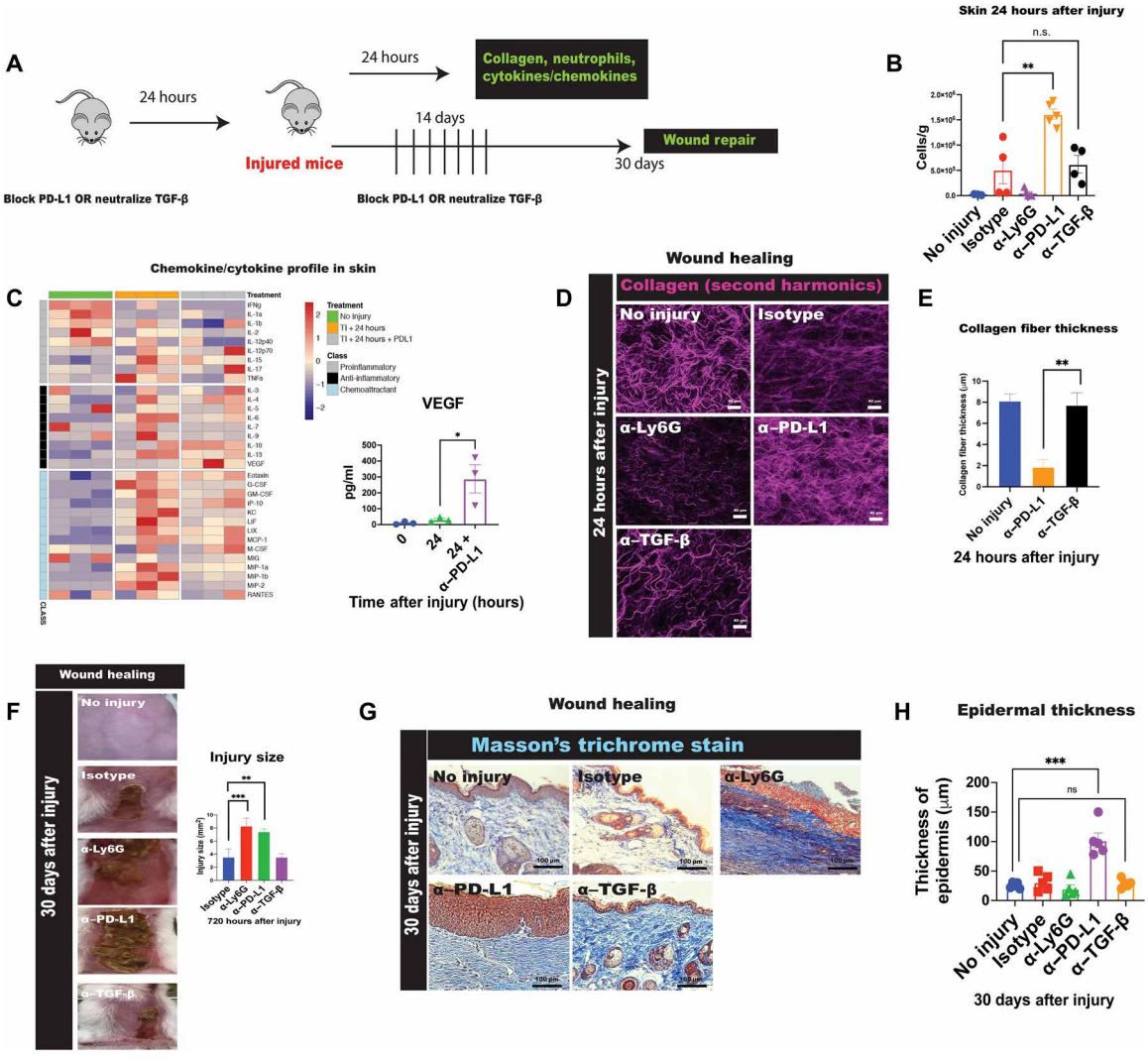

Fig. 7. Blocking PD-L1 perturbs skin healing. (**A**) Schematic representation of how experiments were performed. (**B**) Quantification of neutrophil recruitment to the skin at 24 hours after injury by flow cytometry. (**C**) Overall cytokine/chemokine changes in the skin after PD-L1 treatment. Increased amounts of VEGF in the skin after injury and in PD-L1–treated mice are shown in the bar graph. (**D**) Second harmonic analysis of skin whole mounts 24 hours after injury. (**E**) Quantification of collagen fiber thickness. (**F**) Gross pathological assessment of wound healing. (**G**) Masson's trichrome staining of 5-μm skin sections. (**H**) Quantification of epidermal layer in MTC-stained slides. All experiments were repeated three times ($N = 4$), and representative experiment is presented in the figure. One-way ANOVA with Brown-Forsythe and Welch ANOVA test was performed. Error bars represent SD. α represents what protein the antibody used is targeting. Error bars represent SD. *$P < 0.05$, **$P < 0.05$, and ***$P < 0.0001$.

In our model, we found that neutrophils play a key role in the balance between repair and susceptibility to infection. Upon cutaneous thermal injury, neutrophils are released from the bone marrow. In the bloodstream, neutrophils are stimulated by the presence of TGF-β and begin to express PD-L1. Neutrophils halt in the lung vasculature due to interaction with PD-1 on lung endothelial cells, where increased expression of MMP-9 and Arginase 2 could cause vascular leakage and promote rapid dissemination of bacteria during respiratory infection. Once bacteria enter the bloodstream, although injured mouse neutrophils are able to effectively phagocytose bacteria, they are unable to resolve the infection.

In this work, we bring new light to the dilemma of why our lungs suffer when we undergo injury (*28*). We observe that rapid and robust recruitment of neutrophils to the injury site actually resulted in epidermal overgrowth. Instead, what is required is a slower gated recruitment of neutrophils to the injury site to establish proper healing. It could be that the lung has a gating function during injury, allowing neutrophils to move slowly into the injured site at the cost of lung dysfunction and susceptibility to infection. Reducing neutrophil accumulation in the lung by systemically blocking PD-L1 or neutralizing TGF-β alleviates airway distress and susceptibility to infection, demonstrating how the stopover in the lung is a key mechanism of susceptibility to infection. Conversely, neutrophil recruitment to the injury site seems to require temporal regulation for appropriate healing. In this situation, there can be too much of a good thing. It is likely that depending on the severity and size of the injury, this neutrophil infiltration into the lungs is modulated. Intriguingly, we do find differential roles for anti–PD-L1 versus anti–TGF-β mAbs. In the presence of anti–PD-L1 antibody, neutrophils no longer stop in the lung but move faster to the skin. TGF-β neutralization

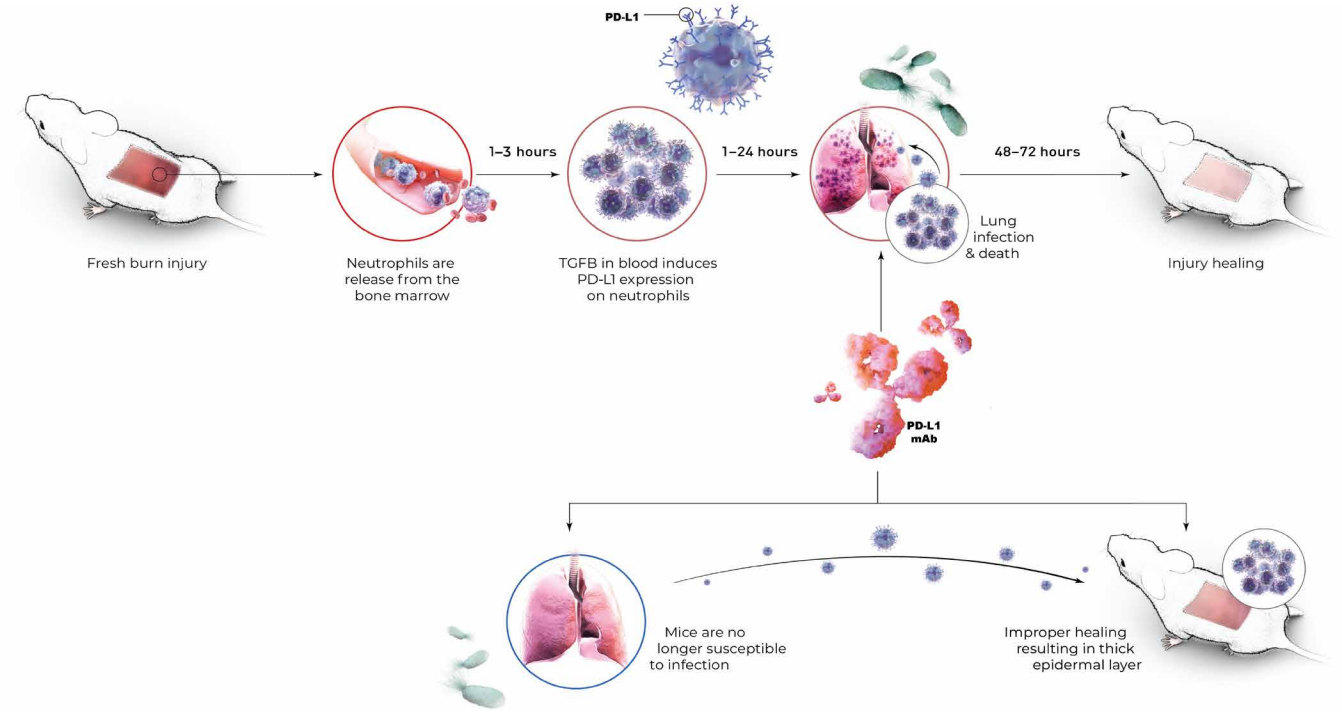

Fig. 8. Risking the lung to save the skin is the way the body regulates regeneration of extensively damaged tissue. Overall schematic of the findings of this study.

also results in reduced neutrophil accumulation in the lung, but in this instance, neutrophil migration to the skin is unchanged. Intriguingly, reduced TGF-β signaling did result in recruitment of excess neutrophils to the bone marrow. Future studies looking closer at the TGF-β–PD-L1 axis signaling cascade are required.

The neutrophil population described here presents an opportunity for the therapeutic modulation of innate immunity following thermal injury. Prior work suggests that these cells contribute to human sepsis more generally; however, additional models of injury are required to confirm a more broad role for PD-L1$^+$ neutrophils and to determine whether the mechanisms described in this communication are common across models of trauma and sepsis (*13*). These data identify TGF-β as a potential therapeutic target capable of preventing ARDS and improving host response to infection following cutaneous thermal injury. Further investigation needs to be performed to better understand these pathways.

MATERIALS AND METHODS

Mouse

Female CF-1 mice between the ages of 8 and 12 weeks were obtained from Charles River. All animal procedures describe here were performed in accordance with federal, state, and institutional guidelines and were approved by the AstraZeneca Institutional Animal Care and Use Committee in an Association for Assessment and Accreditation of Laboratory Animal Care International–accredited facility. Guidelines for humane end points were strictly followed.

Thermal injury procedure

One to 3 days before the injury, mice were shaved and depilated using Nair. The total surface of the back was shaved from the neck to the tail. Mice were administered subcutaneous buprenorphine 30 min before injury. Mice were injured using a device (fig. S1A) set at 92°C that was designed to yield a consistent 12 to 15% total body surface area burn injury. Mice were anesthetized using isoflurane for 10 min before injury and remained on isoflurane for the entire procedure. Distilled H_2O (dH_2O; 0.5 ml) was used to ensure uniform burn injury and was placed on the injury device for 20 s before exposure of animals. Mice were placed on the device in a supine position for 5 s (fig. S1A) one at a time and rapidly removed replacing the 0.5 ml of dH_2O between each animal. After injury, mice were resuscitated with 1 ml of saline interperitoneally.

Bacteria

P. aeruginosa strains 6077 and 6206 were acquired from J.B. Goldberg (Emory). *P. aeruginosa* strain 6206 was made green fluorescence protein (GFP) (6206-GFP) using a plasmid (CTX-Ptac-GFP) that was provided by D. Wozniak (Ohio State) (*24*). Plasmid pPM297 was generated by replacing the GFP coding sequence in CTX-Ptac-GFP with a synthetic gene encoding dsRed2. Both constructs were propagated in *Escherichia coli* JM109. Triparental mating resulting in chromosomal integration of the fluorescent protein expression cassettes was carried out as described previously (*24*). Bacteria were grown overnight on blood agar plates at 37°C. Bacteria were scraped from the plate and suspended in phosphate-buffered saline (PBS). An optical density of 650 nm (OD_{650}) was measured, and bacterial volumes were calculated on the basis of the OD. Bacterial infection and strains: For pneumonia infection, 2.5×10^5 *P. aeruginosa* 6077, 6×10^6 of *K. pneumoniae*, and 1×10^7 of *S. aureus* in a 50-μl suspension were delivered intranasally to mice at various times after injury. For intravenous infections (survival and CFU), 7×10^5 of *P. aeruginosa* 6077 was administered using a 0.1-ml bolus suspended in 0.9% buffered saline. Intravital experiments were performed with 6206-GFP at a dose of 7×10^5.

Flow cytometry

Lungs, liver, skin, spleens, and blood were harvested as previously described (*29*). Mice were euthanized with CO_2. Organs were removed, minced, and placed in 0.5 ml of intracellular fixation buffer (eBioscience) for 2 min while chopping. A total of 4.5 ml of 2% bovine serum albumin (BSA) was then added to the mixture. The lungs (with the mixture) were pressed through a 40-μm strainer using the plunger of a 3-ml syringe, washed with excess volume of 2% BSA (in PBS), and spun down at 500*g* for 10 min at 4°C. Supernatant was discarded. Residual red blood cells were lysed using ACK (ammonium-chloride-potassium) lysis buffer (Gibco) for 5 min. Cells were stained for 20 min with the indicated markers. Cells (from lung or BAL fluid, above) were stained with appropriate antibody cocktails at 4°C (table S1). Blocking antibody (2.4G2, BioXCell) was included in the antibody cocktail. Fluorescence Minus One controls were used when appropriate. Samples were run using FACSymphony flow cytometer (BD) and analyzed using FlowJo software (Tree Star).

Cell sorting

Blood and lungs were collected as soon as possible after thermal injury 30 to 40 min after injury for neutrophil isolation, RNA was extracted from these neutrophils, and microarray was performed. Blood samples were taken into tubes coated with lithium heparin (BD). Three rounds of red blood cell lysis were performed with ACK lysis buffer (Gibco). Samples were stained with antibody cocktailed (table S1) and sorted on BD fusion. Lungs were harvest from mice 30 to 40 min after injury. Lungs were minced in Hanks' balanced salt solution with 1% BSA (Sigma-Aldrich) and strained through a 40-μm nylon filter (BD). Red blood cell lysis was performed on the samples. Samples were stained with antibody cocktail. Gating strategy is depicted in fig. S1F. Samples were sorted using BD fusion machine. Nozzle (100 μm) was used at a flow rate of 2.

Whole-genome microarray

Total RNA was extracted from purified neutrophil populations using the Direct-zol kit (Zymo Research, Irvine, CA). RNA purity and concentration were determined spectrophotometrically. RNA quality was assessed on an Agilent 2100 Bioanalyzer (Agilent Technologies, Santa Clara, CA) using an RNA 6000 Pico LabChip. Total RNA was amplified and labeled using the Nugen Ovation Pico WTA System V2 kit (Tecan Genomics, Redwood City, CA). Affymetrix (Santa Clara, CA) GeneChip Mouse Genome 430 2.0 microarray processing was carried out as outlined in the Affymetrix GeneChip manual. Data capture and initial array quality assessment were performed with the GeneChip operating software. The R statistical analysis tool was used to calculate probe-level summaries (frozen robust multiarray average analysis) from the array CEL files (*30*). All analyses were conducted using R. Pairwise group assessments were conducted for each probeset using a Student's or Welch's *t* test depending on the results of a Bartlett's test for equal variance. Genes were considered differentially expressed if they displayed a fold change >1.5 and unadjusted $P < 0.05$.

Intravital microscopy

Mice were anesthetized [xylazine hydrochloride (10 mg/kg) and ketamine hydrochloride (200 mg/kg)], and the body temperature was maintained at 37°C using a heating pad (CU-201, Live Cell Instrument). The right jugular vein was cannulated to administer fluorescent dyes and additional anesthetic. The trachea of the mouse was exposed, and a small catheter was threaded into the trachea. The catheter was then attached to a small rodent ventilator (Harvard Apparatus). The mouse was placed on its right lateral decubitus position. A small surgical incision was made, and the intercostal muscles between ribs 4 and 5 were gently teased apart forming a ~1.5-cm opening. Intercostal lung window was then carefully placed between ribs 4 and 5. The lung was stabilized with a suction of ~20 mmHg. Images were acquired with a Leica Sp8 upright microscope equipped with a resonance scanner.

Mouse PD-L1 antibody development

PD-L1 antibodies were developed as previously described following immunization (*31*–*33*). Briefly, 6- to 8-week PD-L1 knockout mice (stock no. 32234-JAX) were injected subcutaneously with 20 μg of recombinant murine PD-L1 (mPD-L1) Fc fusion protein (R&D Systems) in Freund's complete adjuvant (Sigma-Aldrich). Three subsequent boosts of 20 μg of recombinant mPD-L1 in Freund's incomplete adjuvant (Sigma-Aldrich) were administered through subcutaneous injection 7, 14, and 22 days after the initial prime. Two days after the fourth boost, a final injection of 20 μg of recombinant mPD-L1 in PBS was administered intraperitoneally. Four days after the last injection, mice were euthanized, and lymph nodes were harvested. Serum antibody blocking was assessed using HTRF assays as previously described (*34*). ***Hybridoma generation.*** Cells were isolated from lymph nodes by mechanical disruption using the gentleMACS dissociator (Miltenyi) and fused with SP2/0 myeloma cells (American Type Culture Collection) using a BTX electrofuser (ECM 2001). Following electrofusion, cells were resuspended in semisolid selection media containing fluorescein isothiocyanate (FITC)–conjugated anti-mouse immunoglobulin G (IgG) monoclonal antibodies [CloneMatrix concentrate (Genetix), Dulbecco's modified Eagle's medium (DMEM) powder (Gibco), 20% fetal calf serum (FCS), 2% GlutaMAX (Gibco), 1% sodium pyruvate (Sigma-Aldrich), 1% penicillin/streptomycin (Gibco), 10% hybridoma cloning factor (Roche), 2% oxaloacetate/pyruvate/insulin (Sigma-Aldrich), 2% hypoxanthine/azaserine (Sigma-Aldrich), goat anti-mouse IgG-FITC (11 μg/ml; BioLegend), goat anti-mouse IgG1-FITC (4 μg/ml; Novus Biologicals), goat anti-mouse IgG2b-FITC (4 μg/ml; Novus Biologicals)]. Media containing cells was divided into Omni Trays (Nunc), and cells were allowed to grow at 37°C under a 7.5% CO_2–enriched atmosphere. Thirtee to 16 days following fusion, IgG-secreting hybridomas were detected and picked into 96-well plates (Costar) containing media [DMEM, 20% FCS, 2% GlutaMAX, 1% penicillin/streptomycin, 10% hybridoma cloning factor, 2% oxaloacetate/pyruvate/insulin, 2% hypoxanthine and thymidine (Sigma-Aldrich)] using the ClonePix robot (Molecular Devices). Hybridomas were allowed to grow for 3 to 7 days before supernatant was harvested from each well using the MiniTrak robot (PerkinElmer). ***cDNA preparation and variable chain sequencing.*** Hybridoma mRNA for heavy- and light-chain variable regions were isolated using Oligo$(dT)_{25}$ magnetic beads (Novagen) in combination with the KingFisher 96 automated magnetic separator (Thermo Fisher Scientific). Contaminating SP2/0 MOPC abVκ mRNA was removed by targeted digestion with RNase H (New England Biolabs) at 37°C for 1 hour. Purified mRNA was transcribed to complementary DNA (cDNA) using SuperScript III reverse transcriptase (Invitrogen) at 44°C for 1 hour and then tailed with poly(G) by incubation with excess dGTP and terminal transferase (New England Biolabs) at 37°C for 1 hour. Variable

light- and heavy-chain genes were amplified using Taq polymerase (Thermo Fisher Scientific) in separate reactions using oligo$(dC)_{25}$ and specific primers to either the CH1 or kappa constant domain. Chain termination method was used to sequence the polymerase chain reaction product. ***IgG purification.*** Selected hybridomas were cultured in serum-free media [HL-1 (Lonza), 2% HybER-Zero (Statins Serum Institute), and 2% GlutaMAX] for 10 days at 37°C under a 7.5% CO_2–enriched atmosphere. IgG was purified from the culture supernatants using either ProPlus or capture select multispecies resin bed Phytips (PhyNexus) on the MiniTrak robot. Absorbance of purified material was read using the EnVision plate reader at 450 nm, and IgG concentration was determined using rat IgG isotype calibration curves.

Enzyme-linked immunosorbent assays

NET formation

ELISAs were used to determine whether thermal injury induced neutrophils to undergo NETosis. To measure NETs, a hybrid of two different ELISA kits was used. Plates were initially coated with anti-elastase capture antibody (R&D Systems). Fresh serum samples were added to the coated wells and then incubated and washed. Next, anti–DNA-POD antibody (Roche) was used to detect DNA in the captured proteins in the wells. Plates were read on SoftMaxPro Plate reader at OD of 405 nm.

Ex vivo phagocytosis analysis

Injured or noninjured mice were intravenously infected with *P. aeruginosa* GFP (strain 6206) at 3 hours after injury. Lungs were harvested 3 hours after infection and prepared for flow cytometry. Neutrophil phagocytosis of bacteria was assessed using Ly6G maker and GFP signal from *P. aeruginosa*.

PD-L1 binding to PD-1

Mouse recombinant PD-1 was used to detect PD-L1 antibody binding. rPD-1 was used to coat 96-well ELISA (Nunc) plates at *x* mcg (micrograms) per well. Coated recombinant PD-1 (rPD-1) plates were blocked followed by evaluating reactivity to anti–PD-L1 mAb that was serially diluted (11 × 3–fold dilutions).

TGF-β ELISA

TGF-β ELISA kit was purchased from Abcam. User manual was followed to quantify TGF-β in serum. Plates were read on SoftMax Pro Plate reader at OD of 450 nm. This kit allows for effective quantification of specifically mouse TGF-β1.

Antibody treatment

Mice were treated with 250 μg of neutralizing or inhibiting antibodies through intraperitoneal injections 24 hours before injury. PD-L1 antibody was made in-house, and anti–TGF-β was purchased from BioXCell (BE0057) and isotype control (BE0083). Once mice were injured and infected, they were treated with antibodies 24 hours after infection. For 30 days of wound healing experiments, mice were administered with neutralizing antibody every other day for the first 2 weeks after injury.

Lung whole-mount staining

Mice were euthanized using CO_2 affixation and perfused with PBS, and lungs were immediately inflated with 2% low-melting point agarose (Life Technologies). Lungs were removed and fixed in 4% paraformaldehyde (Electron Microscopy). Lungs were sectioned at 300-μm slices using a vibratome (Leica). Lungs were permeabilized and blocked using a buffer containing 0.1% Triton X. Samples were blocked with 1% BSA and incubated with Ly6G antibody conjugated to Alexa Fluor 647, CD31 conjugated to Alexa Fluor 488, and PD-1 conjugated to Alexa Fluor 594 overnight at 4°C. Samples were washed five times with permeabilization buffer and mounted on slides.

Skin whole-mount staining

Skin was removed at various time points after injury and fixed in 4% paraformaldehyde for 4 hours. Skins were permeabilized and blocked using a buffer containing 0.1% TritonX-100. Samples were blocked with 1% BSA and incubated with Ly6G antibody conjugated to Alexa Fluor 647 overnight at 4°C. Skins were mounted on glass slides, and Kimwipes soaked in sterile PBS were used to keep the samples from drying. Leica SP8 multiphoton was used to visualize collagen fibers.

Histology and Masson's trichrome staining

Skin samples for histology were fixed in 10% buffered formalin overnight. Samples were then dehydrated and paraffin embedded. Five-micrometer sections were made of the skin for MTC (Masson's trichrome staining) staining. MTC staining was performed as previously described.

Proteomics: Label-free quantitative proteomics analysis

Serum was prepared from whole blood collected after injury and frozen at −80°C before sample processing. Serum depletion was performed using ProteoPrep Albumin and IgG Depletion Kit (MilliporeSigma, St. Louis, MO). Indexed retention time protein developed in-house was spiked into depleted serum as a digestion quality control, and the total protein concentration was measured using the Pierce 660 nm Protein Assay with BSA as a standard (Thermo Fisher Scientific). A total of 150 μg of protein from each sample was processed on the basis of the S-Trap mini digestion protocol with modification (ProtiFi, Farmingdale, NY). In brief, proteins were lysed in buffer composed of 5% SDS and 50 mM triethylammonium bicarbonate (TEAB). Lysed proteins were reduced with 10 mM tris(2-carboxyethyl)phosphine (TCEP) for 15 min at 60°C and alkylated with 40 mM iodoacetamide in the dark for 1 hour at room temperature. Samples were then acidified with phosphoric acid to a final concentration of 1.2%, diluted with seven volumes of S-trap binding buffer, and loaded onto the S-Trap mini spin column. Proteins were digested with mass spectrometry (MS)–grade trypsin/lysC (Promega, Madison, WI) at a 1:50 enzyme:total protein ratio for 1 hour at 47°C. Peptides were eluted in the order of 50 mM TEAB, 0.2% formic acid (FA), and 60% acetonitrile with 0.2% FA. The eluted peptides were combined and fractionated into 12 fractions using Oasis HLB columns (Waters, Milford, MA). The resulting 12 fractions were further concatenated into 4 fractions for liquid chromatography (LC)–tandem MS (MS/MS) analyses.

LC-MS/MS analysis

LC-MS/MS analyses were conducted on an Orbitrap Fusion Tribrid mass spectrometer (Thermo Fisher Scientific) coupled with an UltiMate 3000 RSLCnano System, a Nanospray Flex Ion Source, and stainless steel emitter (40 mm). Sample injections were loaded onto a 2 cm × 75 μm C18 trap column (ReproSil-Pur 120 C18-AQ 7 μm) and a 0.1 mm × 50 cm MonoCap C18 High-Resolution 2000 analytical column (GL Sciences, Tokyo, Japan). The peptides were eluted at a flow rate of 700 nl/min over a 59-min gradient, from 4 to 17% solvent B (38 min), 17 to 34% solvent B (12 min), 34 to 98% solvent B (8.8 min), and 98 to 2% solvent B (0.2 min). Solvent A was composed of 0.15% FA in water with 2% acetonitrile, and solvent B was composed of 0.15% FA in 90% acetonitrile.

The full MS survey scan [*m*/*z* (mass/charge ratio) 375 to 1000] was acquired on an Orbitrap analyzer at a resolution of 120,000 and with a normalized automatic gain control (AGC) target of 187.5%. The maximum injection time for MS scans was 50 ms. MS/MS scans were performed using the linear ion trap with the higher energy

collisional dissociation (HCD) collision energy set to 33%. The ion trap scan rate was set to "rapid," with a normalized AGC target of 200% and a maximum injection time of 50 ms.

Data analysis

MS/MS spectra were analyzed using Proteome Discoverer (version 2.3.0.523; Thermo Fisher Scientific) with the Mascot search engine (version 2.6.0) against the *Mus musculus* database containing 84,239 sequences (UniProt). The search was performed with the following parameters: a maximum of one missed cleavage sites, a tolerance for precursor ion masses of 20 parts per million, and a tolerance for fragment ion masses of 0.8 Da. The static modification settings included carbamidomethyl of cysteine residues. The dynamic modification setting included oxidation of methionine and deamidation of asparagine and glutamine. A false discovery rate of 1% for peptides and proteins was obtained using a target-decoy database search. The quantitative precursor peptide abundance was calculated on the basis of the intensity, and the protein abundance was calculated on the basis of the summed peptide abundance.

Perseus version 1.6.10.50 was used to filter the processed data. Only proteins that were identified and quantified with at least one peptide and in at least 70% of all samples were considered for the analysis. The filtered data were further $\log_2$ transformed and Z score normalized. The identified proteins were evaluated for up- and down-regulation by setting a minimum limit of ±1.5-fold change. Ingenuity Pathway Analysis was used for the enrichment analysis of differentially expressed proteins.

Vascular permeability measurement

Vascular permeability in the lungs was determined using the Evans blue dye extravasation method as described (*27*). Briefly, Evans blue (20 mg/kg; Sigma-Aldrich) was injected intravenously 1 hour before the mice were euthanized. The mice were then perfused with 10 ml of PBS to remove intravascular dye. The lungs were then homogenized in PBS to extract the dye and centrifuged. The absorption of Evans blue was measured in the supernatants at 620 nm and corrected for the presence of heme pigments as follows: A620 (corrected) = actual absorbance at 620 nm − (1.426 × absorbance at 740 nm + 0.03).

Luminex

Thirty-two–plex mouse chemokine/cytokine magnetic bead panel assay was used to analyze BAL fluid (MilliporeSigma, MCYTMAG-70K-PX32). Assays were performed according to the manufacturer's instructions.

Flexivent

Mice were anesthetized with ketamine/xylazine, tracheostomized, and connected to a computer-controlled small-animal mechanical ventilator for mechanical ventilation (200 breaths/min and a tidal volume of 0.2 ml against a positive end-expiratory pressure of 3 cmH_2O). Pressure-volume loop measurements are performed first. This is an extremely important measurement and is diagnostic of a variety of lung parenchymal abnormalities. To measure pressure-volume loops, the lung will be inflated to a particular pressure or volume, and this maneuver will provide important measurements of lung volume, a parameter that is relevant to a variety of respiratory diseases such as asthma and chronic obstructive pulmonary disease. The pressure and flow data obtained during application of each volume perturbation will be used to calculate a complex input impedance of the respiratory system.

Statistical analysis

All experiments were repeated three times, and each figure shows one representative image with four replicates within each group unless otherwise indicated. Statistical analysis was performed using PRISM software (GraphPad). All values are expressed as mean ± SEM unless otherwise indicated in the figure legend. Data were assessed for normal distribution. For two groups, when applicable, unpaired Student's t test (two-tailed) was performed. Otherwise, Mann-Whitney test was performed. When assessing multiple groups, for parametric data, one-way analysis of variance (ANOVA) with Bonferroni's post hoc test was performed. For nonparametric data, Kruskal-Wallis with Dunn's post hoc test was performed. Statistical significance was accepted at $^*P < 0.05$, $^{**}P < 0.001$, and $^{***}P < 0.0001$.

SUPPLEMENTARY MATERIALS

Supplementary material for this article is available at http://advances.sciencemag.org/cgi/content/full/7/10/eabd9436/DC1

REFERENCES AND NOTES

1. A. M. Lachiewicz, C. G. Hauck, D. J. Weber, B. A. Cairns, D. van Duin, Bacterial infections after burn injuries: Impact of multidrug resistance. *Clin. Infect. Dis.* **65**, 2130–2136 (2017).
2. J. Harless, R. Ramaiah, S. M. Bhananker, Pediatric airway management. *Int. J. Crit. Illn. Inj. Sci.* **4**, 65–70 (2014).
3. K. L. Butler, V. Ambravaneswaran, N. Agrawal, M. Bilodeau, M. Toner, R. G. Tompkins, S. Fagan, D. Irimia, Burn injury reduces neutrophil directional migration speed in microfluidic devices. *PLOS ONE* **5**, e11921 (2010).
4. T. A. Spanholtz, P. Theodorou, P. Amini, G. Spilker, Severe burn injuries: Acute and long-term treatment. *Dtsch. Arztebl. Int.* **106**, 607–613 (2009).
5. E. Mathias, M. Srinivas Murthy, Pediatric thermal burns and treatment: A review of progress and future prospects. *Medicines (Basel)* **4**, 91 (2017).
6. Y. Hua, G. Bergers, Tumors vs. chronic wounds: An immune cell's perspective. *Front. Immunol.* **10**, 2178 (2019).
7. M. Phillipson, P. Kubes, The healing power of neutrophils. *Trends Immunol.* **40**, 635–647 (2019).
8. B. McDonald, K. Pittman, G. B. Menezes, S. A. Hirota, I. Slaba, C. C. M. Waterhouse, P. L. Beck, D. A. Muruve, P. Kubes, Intravascular danger signals guide neutrophils to sites of sterile inflammation. *Science* **330**, 362–366 (2010).
9. J. Wang, Neutrophils in tissue injury and repair. *Cell Tissue Res.* **371**, 531–539 (2018).
10. T. Lammermann, P. V. Afonso, B. R. Angermann, J. M. Wang, W. Kastenmüller, C. A. Parent, R. N. Germain, Neutrophil swarms require LTB4 and integrins at sites of cell death *in vivo*. *Nature* **498**, 371–375 (2013).
11. W. Qin, L. Hu, X. Zhang, S. Jiang, J. Li, Z. Zhang, X. Wang, The diverse function of PD-1/PD-L pathway beyond cancer. *Front. Immunol.* **10**, 2298 (2019).
12. N. K. Patil, Y. Guo, L. Luan, E. R. Sherwood, Targeting immune cell checkpoints during sepsis. *Int. J. Mol. Sci.* **18**, (2017).
13. A. C. Patera, A. M. Drewry, K. Chang, E. R. Beiter, D. Osborne, R. S. Hotchkiss, Frontline science: Defects in immune function in patients with sepsis are associated with PD-1 or PD-L1 expression and can be restored by antibodies targeting PD-1 or PD-L1. *J. Leukoc. Biol.* **100**, 1239–1254 (2016).
14. N. K. Patil, L. Luan, J. K. Bohannon, A. Hernandez, Y. Guo, E. R. Sherwood, Frontline Science: Anti-PD-L1 protects against infection with common bacterial pathogens after burn injury. *J. Leukoc. Biol.* **103**, 23–33 (2018).
15. D. Su, H.-I. Tsai, Z. Xu, F. Yan, Y. Wu, Y. Xiao, X. Liu, Y. Wu, S. Parvanian, W. Zhu, J. E. Eriksson, D. Wang, H. Zhu, H. Chen, F. Cheng, Exosomal PD-L1 functions as an immunosuppressant to promote wound healing. *J. Extracell. Vesicles* **9**, 1709262 (2019).
16. J. A. Dingwall, A clinical test for differentiating second from third degree burns. *Ann. Surg.* **118**, 427–429 (1943).
17. R. Rekik, N. Belhadj Hmida, A. Ben Hmid, I. Zamali, n. Kammoun, M. Ben Ahmed, PD-1 induction through TCR activation is partially regulated by endogenous TGF-β. *Cell. Mol. Immunol.* **12**, 648–649 (2015).
18. M. T. Tanita, M. M. Capeletti, T. A. Moreira, R. P. Petinelli, L. T. Q. Cardoso, C. M. C. Grion, Risk factors for acute respiratory distress syndrome in severe burns: Prospective cohort study. *Int J Burns Trauma* **10**, 1–14 (2020).
19. V. Fanelli, V. M. Ranieri, Mechanisms and clinical consequences of acute lung injury. *Ann. Am. Thorac. Soc.* **12** (suppl 1), S3–S8 (2015).
20. W. Li, Eat-me signals: Keys to molecular phagocyte biology and "Appetite" control. *J. Cell. Physiol.* **227**, 1291–1297 (2012).
21. C. Rosales, Neutrophil: A cell with many roles in inflammation or several cell types? *Front. Physiol.* **9**, 113 (2018).
22. K. Pittman, P. Kubes, Damage-associated molecular patterns control neutrophil recruitment. *J. Innate Immun.* **5**, 315–323 (2013).

23. P. Ranganathan, A. Agrawal, R. Bhushan, A. K. Chavalmane, R. Kalathur, T. Takahashi, P. Kondaiah, Expression profiling of genes regulated by TGF-beta: Differential regulation in normal and tumour cells. *BMC Genomics* **8**, 98 (2007).
24. D. Church, S. Elsayed, O. Reid, B. Winston, R. Lindsay, Burn wound infections. *Clin. Microbiol. Rev.* **19**, 403–434 (2006).
25. G. D. Rubenfeld, E. Caldwell, E. Peabody, J. Weaver, D. P. Martin, M. Neff, E. J. Stern, L. D. Hudson, Incidence and outcomes of acute lung injury. *N. Engl. J. Med.* **353**, 1685–1693 (2005).
26. D. R. Principe, A. Park, M. J. Dorman, S. Kumar, N. Viswakarma, J. Rubin, C. Torres, R. M. Kinney, H. G. Munshi, P. J. Grippo, A. Rana, TGFβ blockade augments PD-1 inhibition to promote T-cell-mediated regression of pancreatic cancer. *Mol. Cancer Ther.* **18**, 613–620 (2019).
27. M. Shibuya, Vascular endothelial growth factor (VEGF) and its receptor (VEGFR) signaling in angiogenesis: A crucial target for anti- and pro-angiogenic therapies. *Genes Cancer* **2**, 1097–1105 (2011).
28. A. Kovtun, D. A. C. Messerer, K. Scharffetter-Kochanek, M. Huber-Lang, A. Ignatius, Neutrophils in tissue trauma of the skin, bone, and lung: Two sides of the same coin. *J. Immunol. Res.* **2018**, 8173983 (2018).
29. Y.-R. Yu, E. G. O'Koren, D. F. Hotten, M. J. Kan, D. Kopin, E. R. Nelson, L. Que, M. D. Gunn, A protocol for the comprehensive flow cytometric analysis of immune cells in normal and inflamed murine non-lymphoid tissues. *PLOS ONE* **11**, e0150606 (2016).
30. R Core Team, A language and environment for statistical computing, R Foundation for Statistical Computing, Vienna, Austria (2018).
31. G. Mathis, Probing molecular interactions with homogeneous techniques based on rare earth cryptates and fluorescence energy transfer. *Clin. Chem.* **41**, 1391–1397 (1995).
32. C. N. Pace, F. Vajdos, L. Fee, G. Grimsley, T. Gray, How to measure and predict the molar absorption coefficient of a protein. *Protein Sci.* **4**, 2411–2423 (1995).
33. O. Daramola, J. Stevenson, G. Dean, D. Hatton, G. Pettman, W. Holmes, R. Field, A high-yielding CHO transient system: Coexpression of genes encoding EBNA-1 and GS enhances transient protein expression. *Biotechnol. Prog.* **30**, 132–141 (2014).
34. F. Degorce, A. Card, S. Soh, E. Trinquet, G. P. Knapik, B. Xie, HTRF: A technology tailored for drug discovery - a review of theoretical aspects and recent applications. *Curr. Chem. Genomics* **3**, 22–32 (2009).

Acknowledgments: We thank J. Boyd from the Microscopy Imaging Core Facility, Dynamic Omics, Antibody Discovery and Protein Engineering (ADPE) for the useful advice and training on equipment; R. Rayanki from the Flow Cytometry Core, Dynamic Omics, ADPE; and D. Pao and J. Martinez from the AZ Animal Facility. **Funding:** There is no external funding to report; all work was funded by AstraZeneca. **Author contributions:** A.T. designed and executed the experiments, wrote the manuscript, compiled the data, analyzed the data, performed statistics, and compiled all figures. A.J.C. performed and analyzed the proteomics data. C.M. analyzed the microarray data and Luminex data. M.C. performed thermal injuries. S.H. performed thermal injuries. A.E.K. performed Luminex experiments. A.C.K. developed PD-L1 antibody. C.S.C. performed Klebsiella infection. A.A.B. performed flexiVent assays. N.H. extracted RNA for microarray. V.N.T. performed NET ELISAs. L.C. assessed immunohistochemistry. M.d.l.R. assisted with microarray experiments. M.P. edited the manuscript. A.C.P. edited the manuscript. B.S. edited the manuscript. S.H. edited the manuscript. M.M. developed PD-L1 antibody. C.C.B. edited the manuscript. T.S.C. provided experimental insights, guided the project, and helped write and edit the manuscript. A.D. developed the thermal injury model, edited the manuscript, and assisted in manuscript writing. **Competing interests:** The authors declare that they have no competing interests. C.M., S.H., A.E.K., C.S.C., A.A.B., N.H., V.N.T., L.C., M.d.l.R., M.P., A.C.P., B.S., S.H., M.M., C.C.B., T.S.C., and A.D. are employees of AstraZeneca and may hold stock options in the company. **Data and materials availability:** All data needed to evaluate the conclusions in the paper are present in the paper and/or the Supplementary Materials. Microarray raw data are available in ArrayExpress online database: https://www.ebi.ac.uk/arrayexpress/experiments/E-MTAB-9770/. Additional data related to this paper may be requested from the authors.

Submitted 21 July 2020
Accepted 6 January 2021
Published 5 March 2021
10.1126/sciadv.abd9436

Citation: A. Thanabalasuriar, A. J. Chiang, C. Morehouse, M. Camara, S. Hawkins, A. E. Keller, A. C. Koksal, C. S. Caceres, A. A. Berlin, N. Holoweckyj, V. N. Takahashi, L. Cheng, M. de los Reyes, M. Pelletier, A. C. Patera, B. Sellman, S. Hess, M. Marelli, C. C. Boo, T. S. Cohen, A. DiGiandomenico, PD-L1$^+$ neutrophils contribute to injury-induced infection susceptibility. *Sci. Adv.* **7**, eabd9436 (2021).